



Shear Buckling Stability of Ring Shaped – Steel Plate Shear Walls

Adam R. Phillips¹, Matthew R. Eatherton²

Abstract

Steel plate shear walls (SPSWs) are a lateral load resisting system that utilize the high in-plane shear strength of solid plates. They are typically constructed by welding a thin web plate into the bays of a boundary frame. SPSWs are a popular seismic system because they have high initial stiffness, good ductility, and acceptable hysteretic behavior. However, due to the lack of shear buckling stability of thin web plates, their hysteretic behavior is pinched and the infill panel has negligible stiffness during load reversals. To mitigate these issues, moment resisting connections are required at all the beam to column joints in the boundary frame. Ring shaped – steel plate shear walls (RS-SPSWs) are a novel structural system that offer improved seismic performance by mitigating the buckling related issues of solid web plates.

This paper will present the RS-SPSW concept, development of a plastic strength equation, and a computational study on the shear buckling stability of RS-SPSWs. A modification to the previously derived strength equation is presented in order to improve the equations ability to predict RS-SPSW plastic strength. A computational study was performed using finite element analysis and classical plate theory. Results from the computational study on global shear buckling stability show that RS-SPSWs can achieve their plastic strength before shear buckling. Conversely, solid web plates, at the same web slenderness values, will shear buckle before yielding. A web plate slenderness limit of 100 was found to prevent shear buckling before RS-SPSWs reach their full plastic strength.

1. Background

Conventional Steel Plate Shear Walls (SPSWs) are a prevalent and important lateral load resisting system that are utilized across North America and Japan. Their wide usage can be attributed to their favorable behavior in high seismic areas due to their large initial stiffness, ductility, and acceptable energy dissipation. They can also be thinner in width, quicker to construct, and cheaper to construct than comparable strength concrete shear walls. SPSWs are comprised of a steel infill panel, called a web plate, and a surrounding structural frame. The columns of the structural frame are called vertical boundary elements (VBE) and the beams are called horizontal boundary elements (HBE). Typically, the web plates are constructed out of

¹ Graduate Research Assistant, Virginia Tech, <arp12@vt.edu>

² Assistant Professor, Virginia Tech, <meather@vt.edu>

very thin plate material which undergoes shear buckling at low shear forces and yields along tension field diagonals during seismic activity.

Numerous research projects have explored SPSW behavior in various configurations. Most frequently studied are conventional SPSWs with thin, solid web plates (e.g. Driver et al. 1998; Berman & Bruneau 2003; Sabelli & Bruneau 2006). Other variations of SPSWs explored include web plates with circular perforations (e.g. Vian et al. 2009), web plates with vertical slits (e.g. Hitaka & Matsui 2003), and web plates using low yield point steel (e.g. Vian & Bruneau 2004).

Conventional SPSWs also present several difficulties related to the thin web plates. First, they can be difficult to construct due to welding difficulties and the ease of which they can be damaged on site (Eatherton 2006; Maurya et al. 2013). Second, their flimsy appearance may cause stakeholders, owners or residents, to not trust their seismic resistance (Maurya et al. 2013). Third, the web plates can buckle at relatively small shear loads, possibly during service wind loading. Additionally, shear buckling of the web plates is typically accompanied by loud banging sounds, which if occurred in service, could cause unrest amongst occupants and/or residents. Lastly, while web plate buckling doesn't severely reduce system ductility, it does result in low stiffness and energy dissipation capacity at moderate drift levels. Due to the low stiffness during load reversals, the current design specification requires moment resisting connections at all HBE to VBE joints (AISC 2010). These moment resisting connections improve the hysteretic behavior and energy dissipation capacity of the SPSW system but are expensive to construct (Phillips et al. 2014).

This paper proposes a novel SPSW web plate design, referred to as a Ring Shaped – Steel Plate Shear Wall (RS-SPSW), which mitigates the adverse effects of buckling by utilizing the deformation properties of a ring. RS-SPSWs are characterized by having a web plate with a pattern of ring-shaped cut outs surrounded by a boundary frame free of moment connections. Previous research has shown that RS-SPSWs exhibit more full hysteretic behavior than conventional SPSWs (Egorova et al. 2014; Maurya et al. 2013). Furthermore, RS-SPSWs have more independent variables than conventional SPSWs which allows for tunability of the strength, stiffness, and cyclic performance of the shear wall system.

The following sections discuss the RS-SPSW concept, the computational modeling parameters, the RS-SPSW strength equation, and the shear buckling stability of RS-SPSWs as compared to conventional SPSWs.

2. RS-SPSW Concept & Validation

The RS-SPSW concept exploits the deformation properties of a ring to mitigate buckling. A typical web plate configuration of the RS-SPSW is displayed in Fig. 1. The ring-shaped cut outs in the web plate can be water jet or laser jet cut. The pattern of ring shaped cutouts resists buckling by having its longitudinal elongation approximately equal its transverse shortening. Examining a single rings deformation properties will further explain this phenomenon.

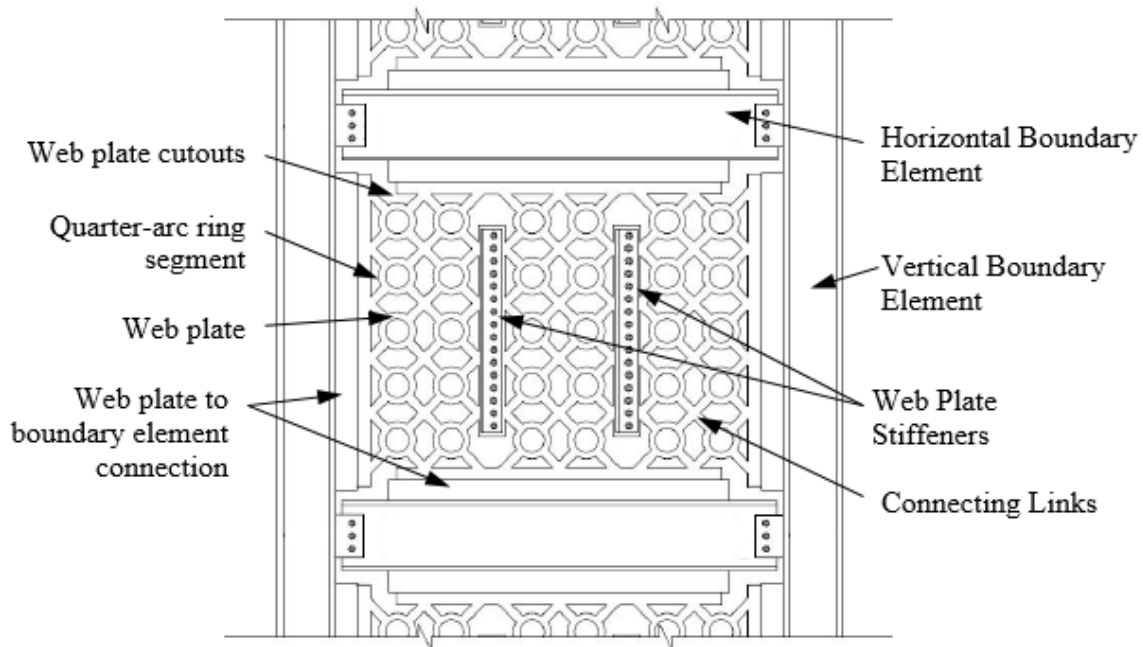


Figure 1: Typical RS-SPSW construction

Consider a single ring from the RS-SPSW panel and an equivalent piece of solid plate from the SPSW panel, shown in Fig. 2a and Fig. 2b. As horizontal shear is applied to the wall it is resisted through a diagonal tension force developed in the ring or solid plate. The diagonal tension force causes an elongation labeled as δ_1 in Fig. 2a and Fig. 2b. For the ring shape it can be shown through geometry, that the transverse shortening, δ_2 , caused by δ_1 is approximately equal to δ_1 . Conversely, for the solid plate the transverse shortening caused by δ_1 is approximately equal to the Poisson's ratio of steel; typically assumed as 0.3 (Maurya et al. 2013). A rings ability to have its transverse shortening equal its longitudinal displacement eliminates the build-up of material in the transverse direction to loading and resists buckling. The exact relationship between δ_1 and δ_2 for a ring and a solid plate is shown in Fig. 2c. For a more details about the deformation geometry of a ring refer to Maurya (2012).

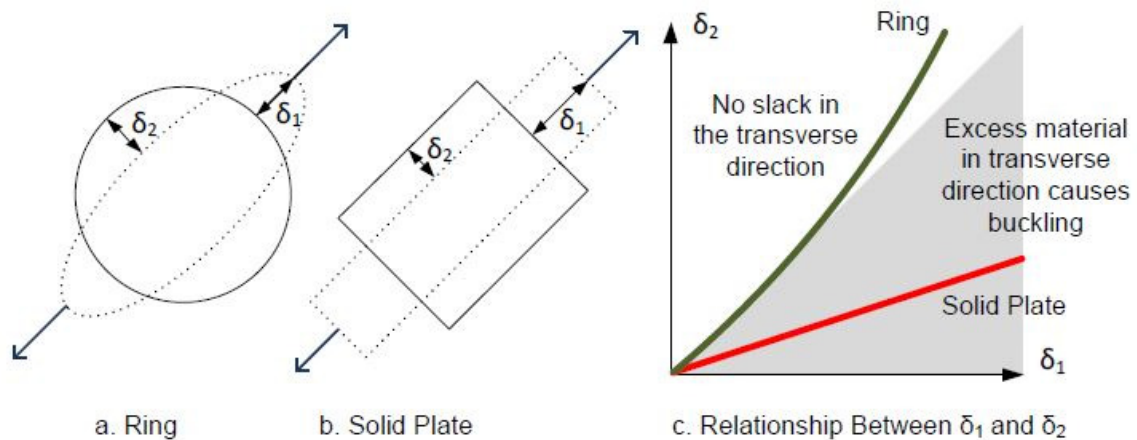


Figure 2: Ring deformation property of equal displacements

The RS-SPSW concept was initially validated through a parametric study utilizing the finite element software Abaqus 6.10 (Simulia 2011). The parametric study yielded a preliminary understanding of the deformation mechanics of the rings and the sensitivity of the wall performance to the geometric parameters (Maurya et al. 2013). The finite element models were one story, one bay representations of the RS-SPSW system with four node reduced integration shell elements (Maurya et al. 2013). The constitutive model utilized monotonic, uniaxial tension coupon data obtained from prior coupon testing of typical 6.35 mm thick A36 steel (Tanamal et al. 2009) with an isotropic hardening rule. The recommended displacement protocol for moment frames from the AISC Seismic Provisions was implemented (Maurya et al. 2013).

The computational study varied the outer ring radius (R_o), ring width (w_c), link width (w_l), and plate thickness (t) to identify their respective local and global effects on panel behavior. Fig. 3 displays the range of parametric study input parameters. Two slenderness values, R_o/t_w and w_c/t_w , are implicitly varied and can be related to the buckling stability of the ring.

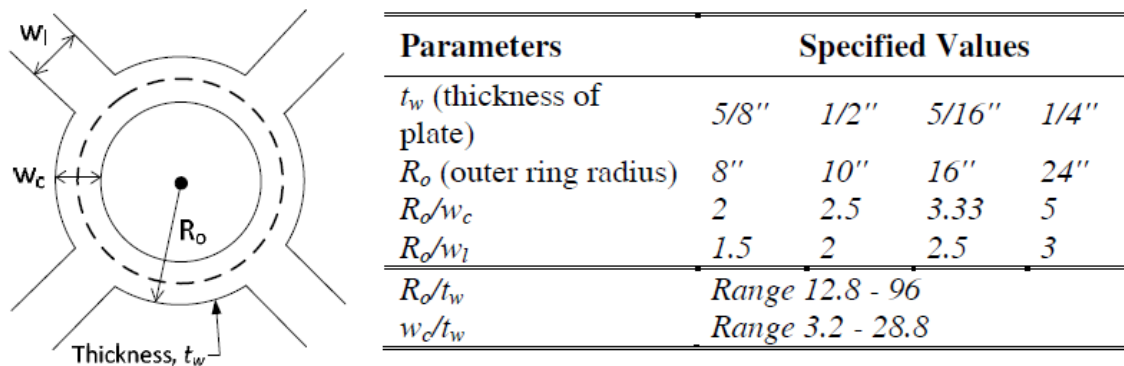


Figure 3: Ring geometric parameters and parametric study input parameters (Maurya et al. 2013)

The computational study revealed that RS-SPSWs present two modes of buckling; global shear buckling and lateral torsional buckling of the rings. The lateral torsional buckling stability of the rings can be controlled by limiting the ring slenderness values. Lateral torsional buckling will not be discussed further in this paper, but additional information will be provided in Phillips & Eatherton (2015). One of the major conclusions from the parametric study was that an increase in plate thickness, t , caused an increase in energy dissipation capacity. It was postulated that this was because an increase in plate thickness decreased strength and stiffness degradation due to plate shear buckling.

Following the parametric study a small-scale experimental program was completed to further validate the concept (Egorova 2013). The test specimens were 914 mm by 914 mm and varied in thickness from 6.35 mm to 12.7 mm. The test setup, shown below in Fig. 4, utilized a vertical hanging MTS 243.60 actuator attached to a "free" column. All the HBE to VBE connections were true pins as to isolate the web plate behavior. The web plate was attached to the boundary elements using double angle, bolted connections. Results from the small-scale experiments led to a recommendation that the web slenderness (h/t) be limited to 100 to prevent shear buckling before the 2% drift cycles (Egorova et al. 2014). For additional information and results of the small-scale experimental regime refer to Egorova (2013) and Egorova et al. (2014).

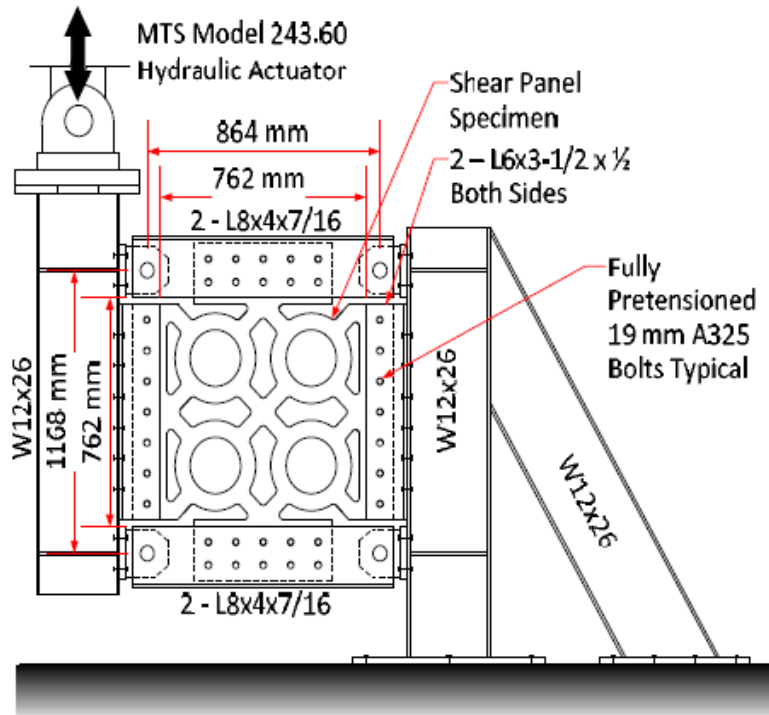


Figure 4: Small-scale experimental test setup (Egorova et al. 2014)

3. Finite Element Models

Finite element models of RS-SPSW web plates were constructed in Abaqus 6.13 to study global shear buckling behavior (Simulia 2011). The models were constructed using four-node reduced integration shell elements. The mesh size varied depending on ring geometry, however for each model at least 6-8 elements were used across the width of a ring. It was found in a previous sensitivity study (not presented here) that the force versus displacement history will converge when using 6-8 elements across the ring width.

An Armstrong-Frederick combined hardening constitutive model was implemented using stress-strain data pairs for the kinematic portion and calibrated hardening parameters for the isotropic portion. The true stress – true plastic strain data pairs, shown in Table 1, for the kinematic backbone curve were taken from previously conducted uniaxial coupon test data on 6.35 mm thick, A36 steel material (Egorova 2013). The 6.35 mm thick material was used during the small-scale experimental program. The isotropic hardening parameters, $Q_{\infty} = 8$ and $b = 3.5$, were calibrated to fit the 6.35 mm thick specimen's experimental hysteretic response.

Table 1: True Stress – True Plastic Strain Pairs for Armstrong-Frederick Material Model

Average True Stress (MPa)	Average True Plastic Strain (mm/mm)
316.0	0.000
330.7	0.005
351.5	0.010
387.0	0.020
416.1	0.030
442.0	0.039
478.2	0.058
503.8	0.077
536.8	0.113
562.0	0.183

An initial imperfection pattern in the shape of the first elastic Eigen buckling mode shape was applied to the web plates at a magnitude of $L/500$. The length, L , used was the shorter dimension of the panel width, a , and the panel height, h . Three panel aspect ratios of 0.5, 1, and 2 were analyzed for global shear buckling, Fig. 5. The panels with an aspect ratio of 1 were 1219 mm by 1219 mm. The panels with an aspect ratio of 2 were 1219 mm by 610 mm and the panels with an aspect ratio of 0.5 were 610 mm by 1219 mm. The outer ring radius, R_o , was kept constant at 102 mm while the ring width, w_c , was varied between 40.6 mm, 50.8 mm, and 67.8 mm. The plate thickness was also varied to achieve web slenderness ratios between 60 and 240.

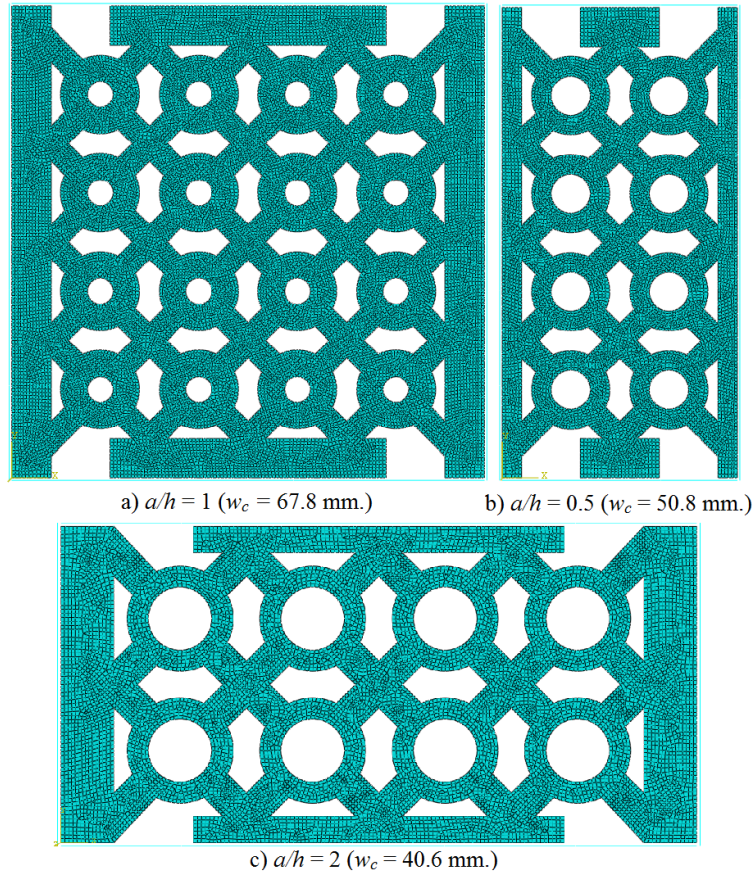


Figure 5: Global buckling study RS-SPSW finite element model aspect ratios

Six additional models were utilized during the strength equation study. These models were constructed in the same manner as the global buckling models but represent future large-scale testing specimens, which are 2667mm by 1727 mm. Table 2 displays their geometric parameters.

Table 2: Additional RS-SPSW models used during strength equation study

Outer Ring Radius, R_o mm.	Ring Width, w_c mm.	Plate Thickness, t mm.	Link Width, w_l mm.	Number of Rings in Row N_r	Ring Proportion Ratio R_o/w_c
152.4	55.9	9.5	76.2	4	2.73
152.4	50.8	12.7	76.2	4	3.00
152.4	48.3	9.5	76.2	4	3.16
111.8	45.7	6.4	55.9	6	2.44
111.8	39.4	9.5	55.9	6	2.84
88.9	31.8	9.5	44.5	8	2.80

The boundary conditions were set to represent the boundary conditions of a full wall. The web plate was surrounded by stiff boundary elements (modeled using frame elements) and was pinned at the plate to boundary element connection. The horizontal to vertical boundary element connections were also pinned as shown in Fig. 6. The base of vertical boundary elements were fixed against x-axis, y-axis, and z-axis displacement (δ_x , δ_y , and δ_z) as well as x-axis and y-axis rotation (θ_x and θ_y). The top of the vertical boundary elements were fixed against z-axis displacement (δ_z) as well as x-axis and y-axis rotation (θ_x and θ_y). The horizontal boundary elements were fixed against z-axis displacement (δ_z) as well as x-axis rotation (θ_x). The displacement protocol was applied at the top left vertical boundary element along the x-axis. Fig. 6 shows the boundary conditions and typical mesh size for a computational model with an aspect ratio of 1 used in the buckling study.

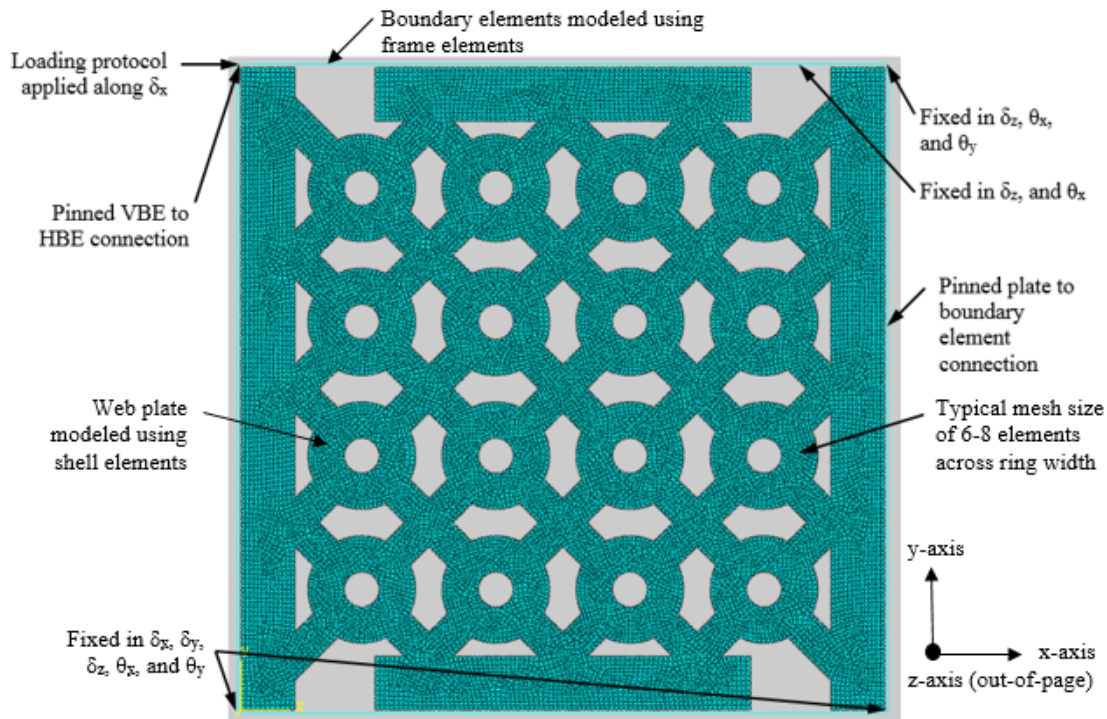


Figure 6: RS-SPSW Computational Model

$$Q = \frac{4M_p}{(R_c - w_l/2)} \quad \text{Eq. 1}$$

$$M_p = F_y \left(\frac{w_c^2 t}{4} \right) \quad \text{Eq. 2}$$

The shear strength of an entire panel is calculated by summing the horizontal component of the ring collapse load for all rings in a row. The rings yield in tension along a 45 degree angle, which is set by the orientation of the connecting links. Eq. 3 is calculated by summing the forces along the horizontal, where $1/\sqrt{2}$ is the $\cos(45)$ and N_r is the number of rings along a row.

$$V_n = \frac{1}{\sqrt{2}} N_r \left(\frac{4M_p}{R_c - w_l/2} \right) \quad \text{Eq. 3}$$

Eight models from the global buckling study and the six models of future large-scale experimental tests were analyzed to see how well Eq. 3 predicted actual yield strength. It was shown that Eq. 3 does an adequate job of predicting the plastic strength for some panels and under predicts plastic strength for others, Fig. 8. This is because Eq. 3 is derived for a ring that has plastic hinges located at the face of the connecting links. The actual strengths were calculated by finding the intercept of the initial stiffness and the tangent stiffness at the peak 0.5% drift cycle. Fig. 8 shows the comparison of predicted strength to actual strength in terms of the non-dimensional ratio of actual collapse load to predicted collapse load. A value of unity signifies a perfect prediction, a value less than one signifies that Eq. 3 over predicts strength (unconservative), and a value greater than one signifies Eq. 3 under predicts strength (conservative). The ring proportion ratio is the ratio of outer ring radius, R_o , to ring width, w_c , and is a measure of the relative ring width.

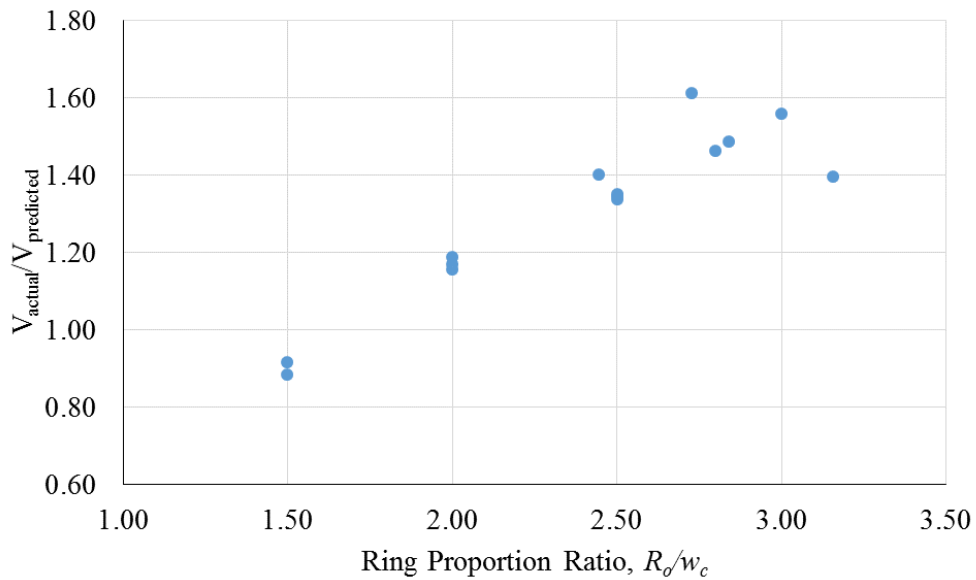


Figure 8: Accuracy of plastic strength equation with center of plastic hinge located at face of link

As shown by Fig. 8, there is an approximately linear relationship between ring proportion ratio, R_o/w_c , and how well the strength equation predicts the collapse load. The average ratio of actual strength to predicted strength for the data set in Fig. 8 is 1.31 and the standard deviation is 0.22. A correction to the strength equation was derived that modifies the location of the center of the plastic hinges. Instead of assuming the center of the plastic hinge is located at the face of the link, the width of the plastic hinge is considered. It also calculates the horizontal and vertical distance between the plastic hinges more accurately by accounting for the curvature of the ring. Fig. 9 shows a diagram of the updated plastic mechanism.

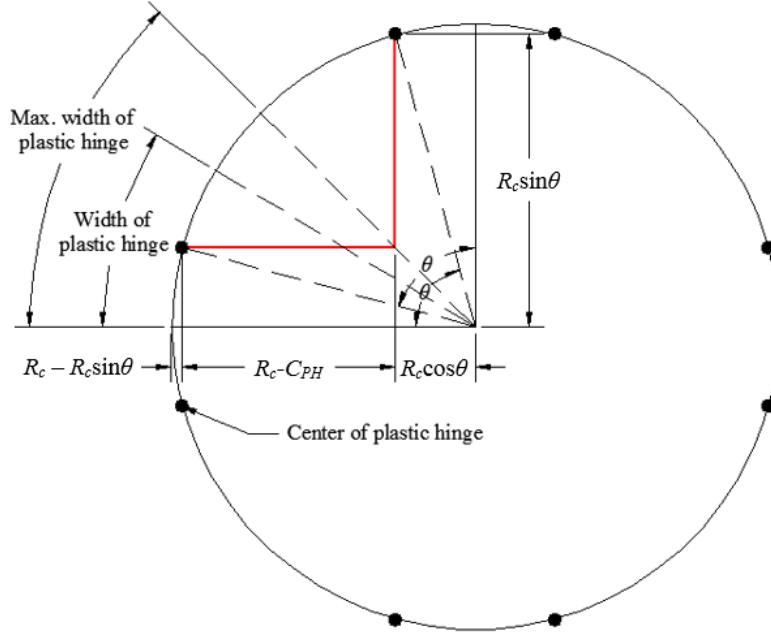


Figure 9: Modified eight hinge ring mechanism using center of plastic hinge

Eq. 4 is the corrected shear strength equation, where C_{PH} accounts for the location of the centerline of the plastic hinge. Eq. 5 and 6 are the equations for how to calculate C_{PH} . Eq. 7 is the equation of the angle θ . The angle θ is bound between $\pi/2$, where there is no influence of the links and the ring yields in a four hinge mechanism, and $3\pi/8$, where the plastic hinge is one eighth of the ring circumference. It is assumed that the width of the plastic hinge varies linearly depending on the ratio of R_o/w_c , which is supported by the computational results (apparent linear variation in Fig. 8).

$$V_n = \frac{1}{\sqrt{2}} N_r \left(\frac{4M_p}{R_c - C_{PH}} \right) \quad \text{Eq. 4}$$

$$C_{PH} = R_c \cos \theta + (R_c - R_c \sin \theta) \quad \text{Eq. 5}$$

$$C_{PH} = R_c (\cos \theta - \sin \theta + 1) \quad \text{Eq. 6}$$

$$\theta = \frac{\pi}{2} - \frac{\pi}{24} \left(\frac{R_o}{w_c} \right) \geq \frac{3\pi}{8} \quad \text{otherwise } \theta = \frac{3\pi}{8} \quad \text{Eq. 7}$$

Fig. 10 shows the effect of the strength equation modification using the same data set as Fig. 8. As shown, the data with R_o/w_c equal to 1.5 is now above the unity line, meaning the strength equation prediction is conservative versus unconservative as it was in Fig. 8. Additionally, the data with R_o/w_c greater than and equal to 2.5 are now closer to the unity line, so their prediction is less conservative and closer to the actual strength. The average ratio of actual strength to predicted strength for the data set in Fig. 10 is 1.18 and the standard deviation is 0.08. The standard deviation being reduced from 0.22 to 0.08 shows that the modified strength equation results in a better prediction of actual strength.

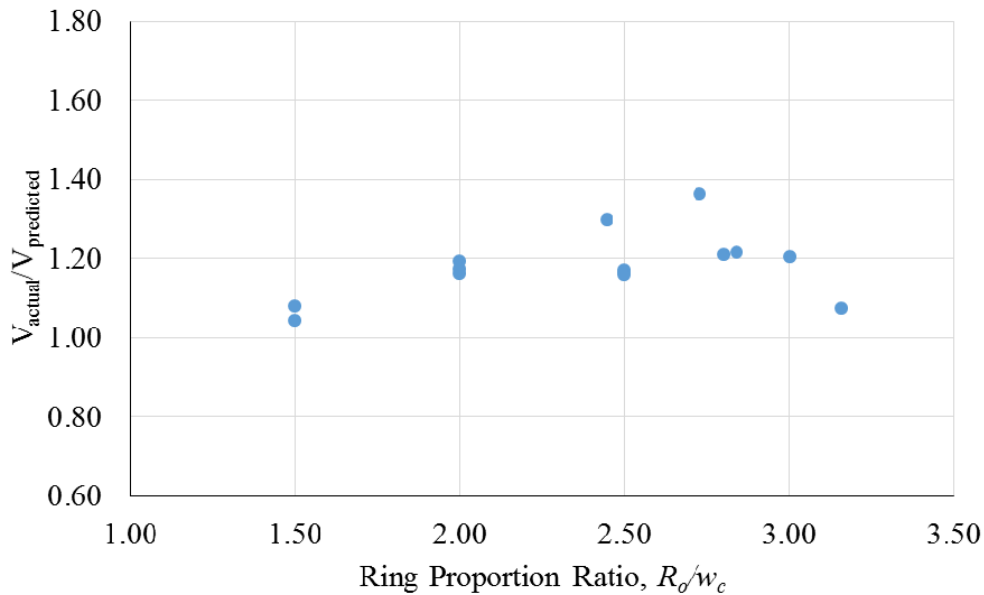


Figure 10: Accuracy of plastic strength equation with center of plastic hinge based on ring proportion ratio

5. Global Shear Buckling

For conventional SPSWs shear buckling of the web plate severely impacts the overall performance of the system. Shear buckling causes the infill panel to lose all stiffness during load reversals until the tension field picks up load in the opposite direction. The loss of stiffness presents itself as pinching in the hysteretic performance of conventional SPSWs. The pinching of the hysteresis also results in less energy dissipation and is the basis of the AISC 341-10 supplementary moment frame requirement.

The underlying challenge to conventional SPSWs with regards to shear buckling is that the buckling load is small relative to the plastic capacity of the plate. Even a very thin plate can have significant shear yield capacity. The theoretical shear buckling stress, τ_{cr} , of solid plates is well established and was originally presented by Timoshenko and Woinowsky-Krieger (1959). Salmon, Johnson, and Malhas (2009) re-formulated the equation to be in terms of the unsupported web plate height, h , and the unsupported web plate width, a , shown in Eq. 8. The

buckling strength, V_{cr} , was calculated by multiplying the elastic buckling stress by the area of the plate, Eq. 9 (Salmon et al. 2009).

$$\tau_{cr} = \frac{\pi^2 E k_v}{12(1 - \mu^2)(h/t)^2} \quad \text{Eq. 8}$$

Where:

$$k_v = 4.0 + 5.34/(a/h)^2 \quad \text{for } a/h \leq 1$$

$$k_v = 4.0/(a/h)^2 + 5.34 \quad \text{for } a/h \geq 1$$

E = Modulus of Elasticity

μ = Poisson's Ratio (0.3 for steel)

$$V_{cr} = \tau_{cr} A_w \quad \text{Eq. 9}$$

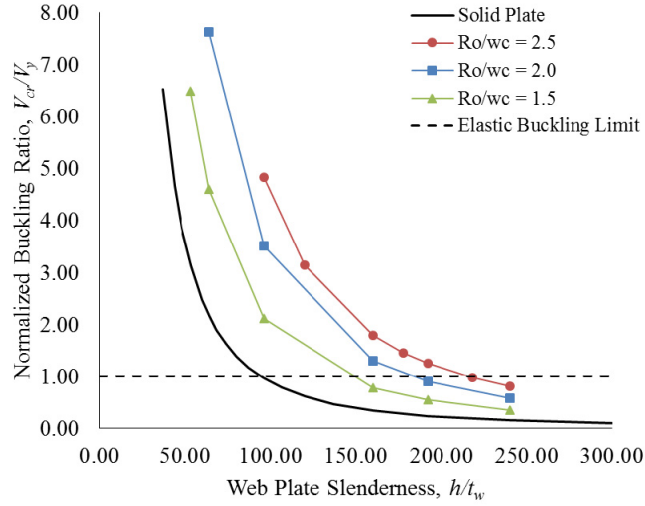
Where:

A_w = Area of solid web plate

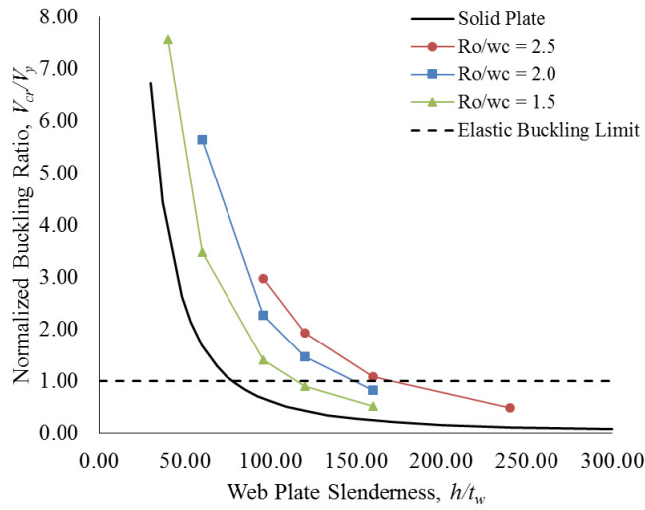
The nominal shear strength, V_n , was calculated as the theoretical shear yield stress, τ_y , multiplied by the web plate area, shown in Eq. 10 (Salmon et al. 2009). The theoretical shear yield stress for a plate is the inverse of the square root of three (approximately 0.6) times the tensile yield strength, F_y .

$$V_y = \tau_y A_w = 0.6 F_y A_w \quad \text{Eq. 10}$$

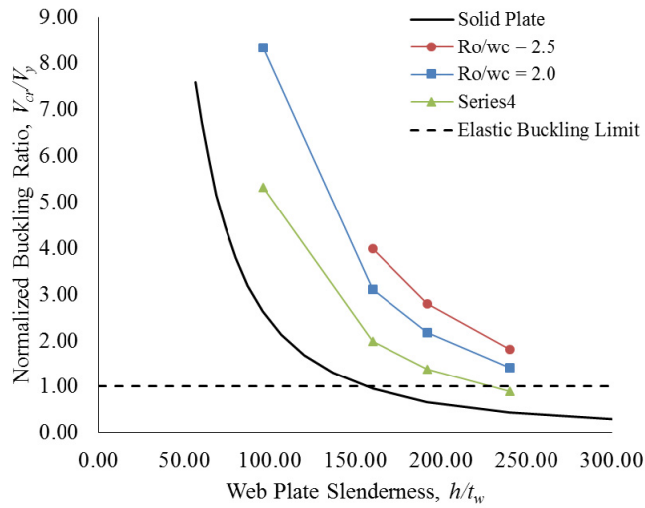
The elastic buckling load for the 42 RS-SPSW model variations in the computational study were found using a linear perturbation analysis in Abaqus. The shear strength of the RS-SPSW panels were calculated using the modified shear strength equation. Fig. 11 plots a normalized buckling ratio of plastic shear strength to elastic buckling strength, V_y/V_{cr} , versus web plate slenderness, h/t , for each of the aspect ratios studied. A normalized buckling ratio greater than one signifies that the plastic shear strength of the plate should be achieved before elastic shear buckling occurs. A normalized buckling ratio less than one signifies that elastic shear buckling will occur before the full plastic strength is achieved. Inelastic buckling of the solid web plates was ignored because it is difficult to determine what an inelastic RS-SPSW buckling mode would be due to the mechanism complexity.



a) Panel aspect ratio (a/h) = 1



b) Panel aspect ratio (a/h) = 2



c) Panel aspect ratio (a/h) = 0.5

Figure 11: RS-SPSW versus solid web plate elastic shear buckling curves

As shown by Fig. 11, the RS-SPSW data points are above the solid plate curve. This causes the web slenderness value at the intersection with the elastic buckling limit (buckling ratio = 1.0) for a RS-SPSW to be greater than for a solid plate. A bigger web slenderness value means the RS-SPSW plate can be more slender and still reach its plastic strength before elastic shear buckling. This proves that the RS-SPSW concept can significantly reduce shear buckling of web plates as compared to conventional SPSWs with the same web slenderness value. It is proposed, based on Fig. 11, that the web slenderness should be limited to 100 to eliminate shear buckling for any RS-SPSW configuration with an aspect ratio between 0.5 and 2. This limit was originally proposed in Egorova et al. (2014) and was further validated by this computational study

The RS-SPSW concept improves shear buckling resistance in two ways. First, it utilizes the equal deformation property of a ring where the longitudinal elongation is approximately equal to the transverse shortening. This property is activated after the ring forms a plastic mechanism and is therefore not reflected in the analysis presented here. Second, by removing material from a solid plate, the RS-SPSW drastically decreases its yield strength while only moderately effecting its elastic buckling load. By significantly decreasing the yield strength, V_y , while keeping the elastic buckling strength, V_{cr} , relatively constant, the RS-SPSW increases the normalized buckling ratio. Fig. 12 shows a plot of yield strength versus elastic critical buckling strength for different web slenderness. All models on this plot have an aspect ratio of 1. Points to the left of the elastic buckling line have a buckling ratio of greater than 1.0.

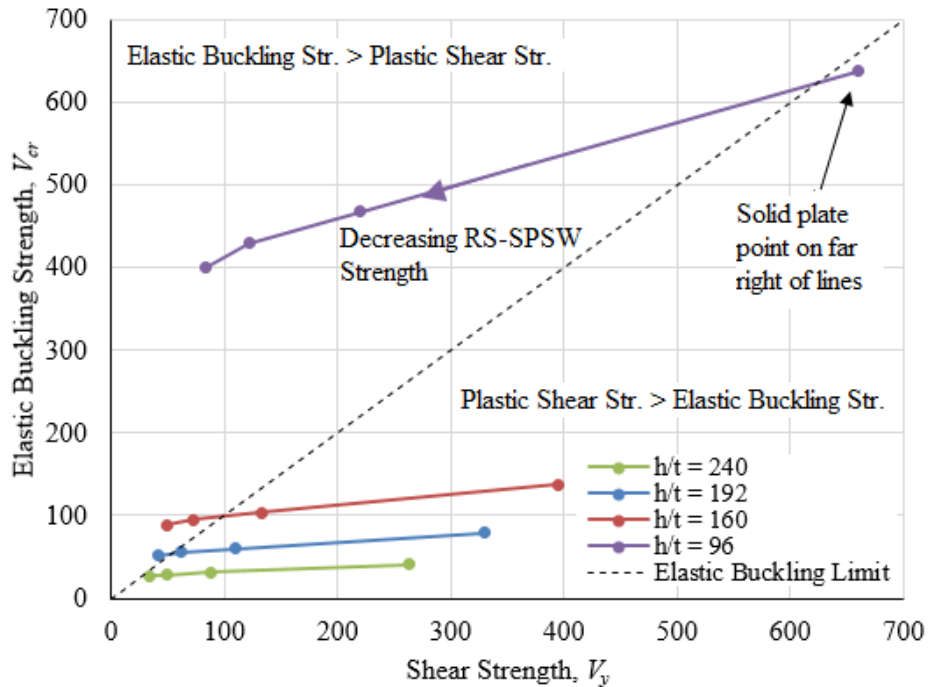


Figure 12: Decreasing RS-SPSW strength with approximately constant elastic buckling strength

Fig. 12 shows that for any given web slenderness, h/t , the RS-SPSW improves the elastic buckling stability by significantly decreasing the plastic shear strength. As the plastic shear strength decreases it starts to control the behavior. Once the shear strength is smaller than the elastic critical buckling load the web plate will form a plastic mechanism without elastic shear buckling.

6. Conclusions

The RS-SPSW system improves conventional SPSW cyclic performance by eliminating buckling. This paper presented a computational study that examined the RS-SPSW strength equation and global shear buckling stability. The computational models included both material and geometric nonlinearities. A modification was proposed for the strength equation that incorporates the width of the plastic hinge in the plastic mechanism. This modification was shown to significantly improve the strength equations ability to predict the web plate plastic strength. It was shown that RS-SPSWs offer improved global shear buckling stability when compared to conventional solid web plates. It was proposed that to prevent global shear buckling as a limit state the web slenderness ratio, h/t , should be less than 100. Using the updated strength equation in conjunction with the web slenderness limit makes it possible to design a RS-SPSW system that does not elastically shear buckle.

Acknowledgments

The authors would like to acknowledge the support from AISC through the Milek Faculty Fellowship Program.

References

- ABAQUS Version 6.13 Documentation, Dassault Systems, 11, Rue Marcel Dassault, 78140 Velizy Villacoublay, France.
- AISC (2010). "Seismic provisions for structural steel buildings." *ANSI/AISC 341-10*, American Institute of Steel Construction, Inc., Chicago, IL.
- Berman, J., and Bruneau, M. (2003). "Plastic analysis and design of steel plate shear walls." *Journal of Structural Engineering*, 129(11), 1448-1456.
- Driver, R. G., Kulak, G. L., Elwi, A. E., and Kennedy, D. J. (1998). "Cyclic test of four-story steel plate shear wall." *Journal of Structural Engineering*, 124(2), 112-120.
- Eatherton, M. R. (2006). "Design and construction of steel plate shear walls." *Proceedings of the Eighth U.S. National Conference on Earthquake Engineering*, April 18-22, San Francisco, CA.
- Egorova, N. (2013). "Experimental study of ring-shaped steel plate shear walls." Master's Thesis, Virginia Tech, Blacksburg, VA.
- Egorova, N., Eatherton, M. R., and Maurya, A. (2014). "Experimental study of ring-shaped steel plate shear walls." *Journal of Constructional Steel Research*, 103(2014), 179-189.
- Hitaka, T., and Matsui, C. (2003). "Experimental study on steel shear walls with slits." *Journal of Structural Engineering*, 129(5), 586-595.
- Maurya, A. (2012). "Computational simulation and analytical development of buckling resistant steel plate shear wall (BR-SPSW)." Master's Thesis, Virginia Tech, Blacksburg, VA.
- Maurya, A., Egorova, N., and Eatherton, M. R. (2013). "Development of ring-shaped steel plate shear walls." *Proceedings of the 2013 ASCE Structures Congress*, May 2-4, Pittsburg, PA. 2971-2982.
- Phillips, A. R., and Eatherton, M. R. (2015). "Ring Shaped – steel plate shear wall lateral torsional buckling behavior." *Proceedings of the 2015 ASCE Structures Congress*, May 23-25, Portland, OR.
- Phillips, A. R., Eatherton, M. R., and Koutromanos, I. (2014). "Ring shaped – steel plate shear walls for improved seismic performance." *Proceedings of the SEAOC 83rd Annual Convention*, September 10-14, Indian Wells, CA.
- Sabelli, R. and Bruneau, M. (2006) "Design Guide 20: Steel Plate Shear Walls." *AISC DG20*, American Institute of Steel Construction, Inc., Chicago, IL.
- Salmon, C., Johnson, J., and Malha, F. (2009). *Steel Structures Design and Behavior*, 5th Ed., Pearson Prentice Hall, New Jersey.
- Tanamal, A., Eatherton, M., and Hajjar, J. F. (2009). "Controlled rocking of steel-framed buildings with replaceable energy dissipating fuses fuse material coupons – tension tests." *Tech. Rep. 61801*, University of Illinois at Urbana-Champaign, Urbana, IL.
- Timoshenko, S. and Woinowsky-Krieger, S. (1959). *Theory of Plates and Shells*, 2nd Ed., McGraw-Hill Book Company, New York.

- Vian, D., and Bruneau, M. (2004). "Testing of special LYS steel plate shear walls." *Proceedings of the 13th World Conference on Earthquake Engineering*, August 1-6, Vancouver, B.C., Canada.
- Vian, D., Bruneau, M., Tsai, K. C., and Lin, Y. C. (2009). "Special perforated steel plate shear walls with reduced beam section anchor beams I: Experimental investigation." *Journal of Structural Engineering*, 135(3), 211-220.